Fluorescent reconstitution on deposition of $PM_{2.5}$ in lung and extrapulmonary organs

Donghai Li (李东海)[a], Yongjian Li (李永健)[a], Guiling Li (栗桂玲)[b], Yu Zhang (张宇)[c], Jiang Li (李疆)[d], and Haosheng Chen (陈皓生)[a,1]

[a]State Key Laboratory of Tribology, Tsinghua University, 100084 Beijing, China; [b]School of Pharmaceutical Sciences, Tsinghua University, 100084 Beijing, China; [c]School of Medicine, Tsinghua University, 100084 Beijing, China; and [d]School of Mechanical Engineering, University of Science and Technology, 100083 Beijing, China

Edited by David A. Weitz, Harvard University, Cambridge, MA, and approved December 24, 2018 (received for review October 23, 2018)

The deposition of $PM_{2.5}$ (fine particulate matter in air with diameter smaller than 2.5 μm) in lungs is harmful to human health. However, real-time observation on the deposition of particles in the acinar area of the lung is still a challenge in experiments. Here, a fluorescent imaging method is developed to visualize the deposition process with a high temporal and spatial resolution. The observations reveal that the deposition pattern is nonuniform, and the maximum deposition rate in the acinar area differs significantly from the prediction of the widely used average deposition model. The method is also used to find single particles in the kidney and liver, though such particles are commonly believed to be too large to enter the extrapulmonary organs.

$PM_{2.5}$ | lung | air pollution | particle deposition | extrapulmonary organs

Particulate matter (PM), a component of air pollutants with an aerodynamic diameter smaller than 10 μm, can be inhaled and deposited in the lungs. The deposition of PM in the lungs will cause pulmonary injuries such as asthma, pulmonary dysfunction, pneumonia, and lung cancer (1–4). When the particles are smaller than 2.5 μm ($PM_{2.5}$), they can reach the terminal bronchioles and enter alveoli, which is harmful to the respiratory system. For example, the morbidity of lung cancer increases 36% for every increment of 10 $\mu g/m^3$ $PM_{2.5}$ in the air (5). Furthermore, finer particles (nanoparticles) can pass through the air-blood barrier in the acinar region and enter the blood circulation, inducing injury in the extrapulmonary organs (6–8). Knowing the precise deposition process and the transport mechanism of inhalable particles is crucial for studies of the health risk assessment in air pollution and drug delivery in the lung (9).

The deposition process has been studied for decades, and a thorough investigation on the deposition of particles is provided in the report by the International Commission on Radiological Protection (ICRP) (10). Based on the experimental data collected in the report, an ICRP model has been built to evaluate the deposition of particles from 1 nm to 10 μm in distinct anatomical regions in lungs, and the model has been widely used in studies of the health effects of air pollution (11, 12). The model is established on the assumption that the particles deposit uniformly in each generation of the airway in lungs. However, the deposition process and patterns are affected by the particle size. According to current understanding, kinematics of particles in the acinar region are dominated by the gravitational sedimentation for large particles (larger than 2.0 μm), while Brownian motion influences small ones (smaller than 0.1 μm) (13, 14). For intermediate particles in the size range of 0.1–1 μm, transport is dependent on the local irreversible kinematics within the alveolar cavities (13, 15–17). Because of the different kinematics, the deposition process and patterns are more complicated than those predicted by the average model based on uniform deposition. This raises an important question: How can we know the real deposition rate in a local acinar region when the deposition pattern is nonuniform? It is still a challenge to measure the pulmonary deposition of particles in vivo. Radiolabeled particles are commonly used, but the spatial resolution is too coarse to distinguish and count the particles in a local area (10, 18). High-resolution deposition patterns in a lung can be obtained, but only from visualization in killed animals (19). Therefore, there is an urgent demand for a real-time measurement in vivo with high resolution both in time and in space.

In this work, inhalation experiments are performed in vivo to obtain the deposition patterns and the deposition rates of the particles in local areas of a mouse lung using a fluorescent imaging method. Fluorescent polystyrene latex microspheres with the sizes of 0.2 μm ($PM_{0.2}$) and 2 μm ($PM_{2.0}$) are used, respectively, to simulate the small and large components of $PM_{2.5}$ in the air. The concentrations of the particles in the air are 17.5, 175, and 1,750 $\mu g/m^3$, corresponding, respectively, to the air quality levels of good, high pollution, and ultra-high pollution conditions according to National Ambient Air Quality Standards (NAAQS, 1997). The deposition of the particles in lungs are observed by a two-photon imaging microscope through a small surgical incision in the rib cage, and the deposition rates of particles in local areas are measured from the images in time sequence. The experimental details are provided in the *Materials and Methods* section. The images of the particles and the variation of the PMs levels are provided in *SI Appendix*, Figs. S1 and S2.

Results

Deposition Patterns. The deposition patterns of the $PM_{0.2}$ and $PM_{2.0}$ particles in the acinar regions are investigated first before we choose a local area to measure the deposition rate. The frozen sections of the lung are made along the sagittal plane after the inhalation experiments, and the fluorescent deposition patterns of the $PM_{2.0}$ and $PM_{0.2}$ are shown in Fig. 1 *A* and *B*, respectively.

Significance

It is always a challenge to see the deposition of single $PM_{2.5}$ particles, the harmful inhalable aerosols in the polluted air, in alveolar region, and their invasion to the extrapulmonary organs. The dynamic deposition process and the nonuniform deposition pattern of $PM_{2.5}$ in the alveolar region are revealed using a fluorescent imaging method with high temporal and spatial resolutions. This observation technology would also bring insight in the study of the public health in air pollution and lung administration.

Author contributions: J.L. and H.C. designed research; D.L. performed research; H.C. contributed new reagents/analytic tools; Y.L., G.L., Y.Z., and H.C. analyzed data; and J.L. and H.C. wrote the paper.

The authors declare no conflict of interest.

This article is a PNAS Direct Submission.

[1]To whom correspondence should be addressed. Email: chenhs@tsinghua.edu.cn.

This article contains supporting information online at www.pnas.org/lookup/suppl/doi:10.1073/pnas.1818134116/-/DCSupplemental.

Published online January 28, 2019.

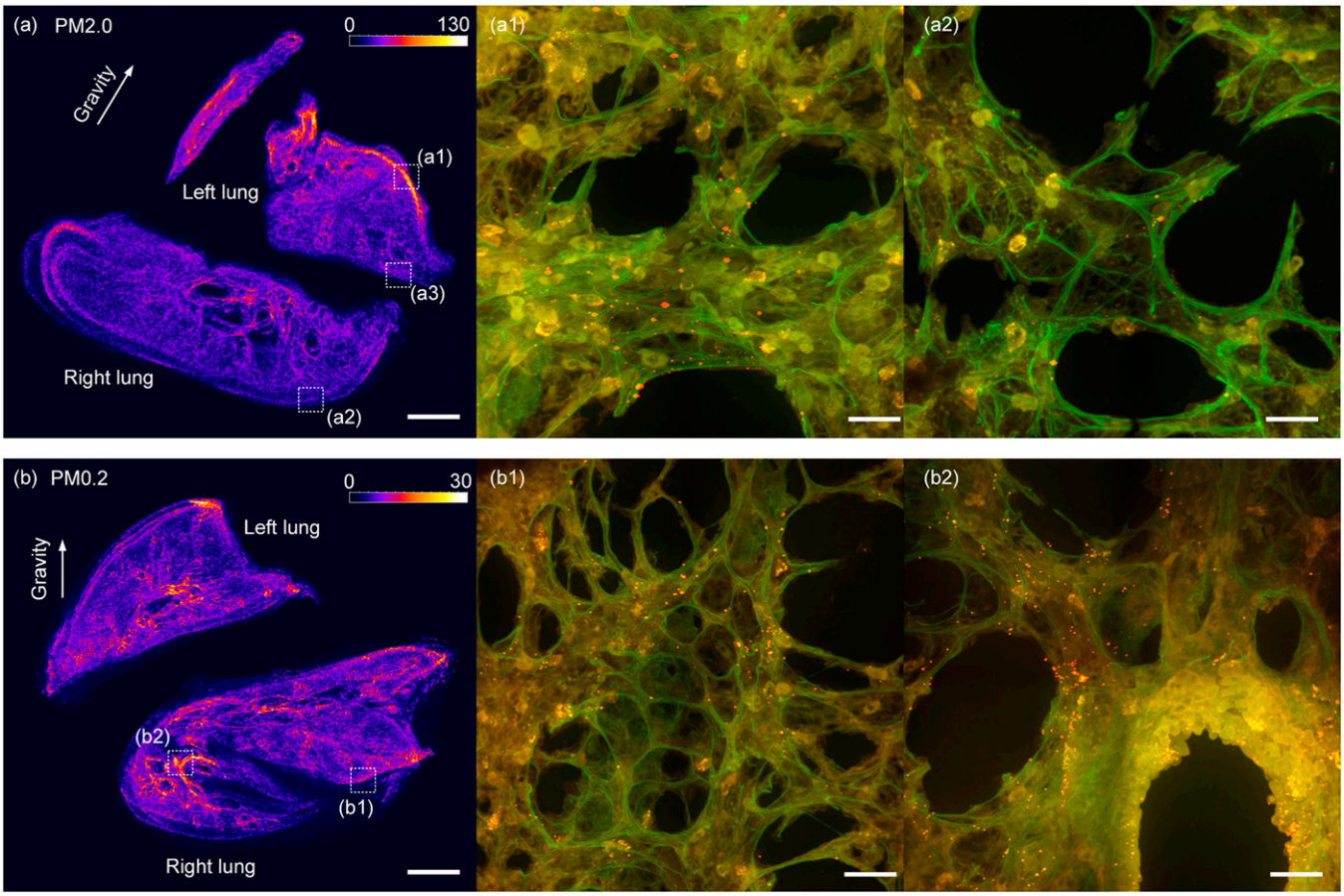

Fig. 1. The fluorescent deposition patterns of $PM_{2.0}$ and $PM_{0.2}$ particles in lungs. *A* and *B* are the deposition patterns of $PM_{2.0}$ and $PM_{0.2}$ in a mouse lung by the fluorescent intensity, respectively. *A1* and *A2* show the high and low concentrations of $PM_{2.0}$ particles in two local areas at the left and right edges, respectively, of a mouse lung. (*B*) A more uniform deposition pattern of $PM_{0.2}$ in the lung with equivalent fluorescent intensity on the left and right edges of the lung. (*B1*) There are still a lot of $PM_{0.2}$ particles in a local acinar area at the right edge of the right lung. (*B2*) More $PM_{0.2}$ particles deposit in the bronchiole region. The red and the orange dots in *A1*, *A2*, *B1*, and *B2* are fluorescent $PM_{2.0}$ particles. (The scale bars in *A* and *B* are 1 mm, while in the other four images are 20 μm.)

The deposition pattern of $PM_{2.0}$ is found to be nonuniform in the lung according to the variation of the fluorescent intensity as shown in Fig. 1*A*. The particles aggregate at the edge of the left lung and form a high-concentration area. A local region (a1) marked with the dash square in the high-concentration area is observed at higher magnification, where a lot of red and orange fluorescent particles are found, as shown in Fig. 1*A1*. On the contrary, $PM_{2.0}$ has a much lower concentration on the opposite side of the edge of the lung. A local low-concentration region (a2) in the dash square is observed at higher magnification, and only a few fluorescent particles are found, as shown in Fig. 1*A2*. This kind of nonuniform deposition patterns of the $PM_{2.0}$ in lungs appear in all mice in the experiments, and it is attributed to the effect of gravitational sedimentation on large particles. According to the current understanding, the large particles aggregate along the lowest place of the lung under the influence of the gravitation force, while in the experiment the lowest place is the edge of the left lung of the mouse because the mouse is lying on its left side.

Compared with $PM_{2.0}$, $PM_{0.2}$ has a more uniform deposition pattern in the acinar region. For example, there is still a medium fluorescent intensity at the right edge of the right lung. A local area in this region marked with the dash square (b1) is observed at higher magnification, and a lot of particles are seen, as shown in Fig. 1*B1*. The uniform deposition pattern of $PM_{0.2}$ in the acinar region indicates that the gravitational force is not the main factor that influences the motion of the smaller particles. The kinetics of the $PM_{0.2}$ is largely affected by the local unsteady airflow patterns within alveolar cavities, where the particle is diverted from an escape zone to a capture zone (or vice versa) (13, 15–17). Additionally, the highest concentration of $PM_{0.2}$ is in the bronchiole region, a local area marked with the dash square (b2) is observed, and more particles are found on the surface of the bronchiole, as shown in Fig. 1*B2*.

Deposition Rates. Since $PM_{2.0}$ has a nonuniform deposition pattern in the acinar region, its deposition rate in local areas may differ significantly from the average value in the whole region, and the real deposition rate in a local area needs to be measured separately. To determine the deposition rate of $PM_{2.0}$ particles in the acinar region, two typical local areas for observation are chosen. One is from the high-concentration region at the left side of the left lung, such as area (a1) in Fig. 1*A*, which represents the region with the maximum deposition rate, and the other is from the medium concentration region at the right side of the left lung, such as area (a3) in Fig. 1*A*, which represents the region with an average deposition rate. The measurement of the deposition rate in the selected region is always a challenge in experiments because of the difficulties in the visualization of the microscale particles in a breathing lung. Here, the deposition process of the particles is visualized in a time sequence using a two-photon imaging microscope in an inhalation experiment in vivo assisted by a ventilator. The lung is gently immobilized and the observation area in the lung is scanned with the microscope from the bottom to the top in 20 s. For each scan, there are 12 layers with the

interval of 2 μm, and the time interval between the two consecutive scans is 30 s. The deposited particles in the scanned images can be recognized according to their fluorescence, and the number of the particles in the observation area is acquired. Therefore, real-time observation on the deposition process of particles in the acinar region is realized and the deposition rate in a local area can be measured in short time intervals. The details of the experiment are provided in the *Materials and Methods* section.

The deposition process of $PM_{2.0}$ in a local area in the high-concentration region is shown in Fig. 2. In the images, the tissue is in green color under the exciting light, while the emission light of fluorescent particles is red. When fluorescent particles are located at the place where the green light of the tissue is strong, they will present yellow color. Therefore, the red and yellow dots in the images are both recognized as the $PM_{2.0}$ particles.

At the beginning of the experiment, there are no fluorescent particles in the acinar region, and only the porous structure of the acinar region is seen in green color, as shown in Fig. 2*A*. When fluorescent particles are ventilated into the lung, they are found in the observation area and gradually deposit in the area. The deposition pattern of $PM_{2.0}$ at 5 min during the ventilation is shown in Fig. 2*B*. At the end of the ventilation at 15 min, clean air containing no $PM_{2.0}$ particles is pumped into the lung. Some of the deposited particles are found to be removed from the area, while most of them are still left, as shown in Fig. 2*C*. This inhalation experiment assisted by the fluorescent imaging method realizes a real-time observation on the deposition process of the particles in a local area in the acinar region with high resolution both in time and in space. Thus, the deposition process of $PM_{2.0}$ in the deep pulmonary acinus can be quantitatively measured over time, and the deposition of single particles in a short exposure time can also be detected.

The number of the $PM_{2.0}$ in the selected local area is acquired from the reconstructed 3D image as shown in Fig. 3*A*. The 3D image helps to distinguish the deposited particles in case some of them are missed in the 2D images. The number of the particles deposited in the local area selected from the high-concentration region and that in the local area selected from the medium concentration region are compared in Fig. 3*B*. The number of particles in each kind of area is from five mice. In Fig. 3*B*, the number of the deposited particles in the high-concentration region (max.) is obviously higher than that in the medium concentration region (avg.). It validates that the two local areas have distinct deposition rates, and the fluorescent imaging method is effective to be used to study the nonuniform deposition of particles in the acinar regions.

With the counted number of the particles deposited at the different exposure times as shown in Fig. 3*C*, the maximum (max.) deposition rate in the high-concentration area and the average (avg.) deposition rate in the medium concentration area are acquired. In the figure, the number of the particles deposited in the local area is recognized to have a linear relationship with the exposure time. According to the fitted lines in Fig. 3*C*, the maximum deposition rate of $PM_{2.0}$ (U_N) is 0.8/min, while the average deposition rate is 0.2/min. Consequently, the mass deposition rate (U_m) can be expressed as $U_m = U_N \times V_p \times \rho/V_{tg}$, where V_p is the volume of the particle, ρ is the density of the particles, 1.05 g/mL, V_{tg} is the volume of the selected local area, $210 \times 210 \times 24$ μm^3. With the measured value of U_N, the maximum deposition rate of $PM_{2.0}$ is 3.5 $\mu g \cdot min^{-1} \cdot ml^{-1}$, while the average deposition rate of $PM_{2.0}$ is 0.7 $\mu g \cdot min^{-1} \cdot ml^{-1}$. Thus, there is a significant difference between the average and the maximum deposition rates of the $PM_{2.0}$ particles in the acinar region in a lung.

This measured deposition rates are compared with the prediction value according to the widely used average deposition model (10). The total $PM_{2.0}$ mass inhaled into the lung is 1,750 ($\mu g/m^3$) × 0.2 (ml/breath) × 120 (breath/min), while the total volume of the acinar region of a mouse used in the experiment is $\sim 10 \times 10^{-3}$ ml. According to the ICRP model, $PM_{2.0}$ have ~10% deposition percentage in the alveoli region, and the calculated mass deposition rate is 0.42 $\mu g \cdot min^{-1} \cdot ml^{-1}$. The measured maximum and average deposition rates are compared with the

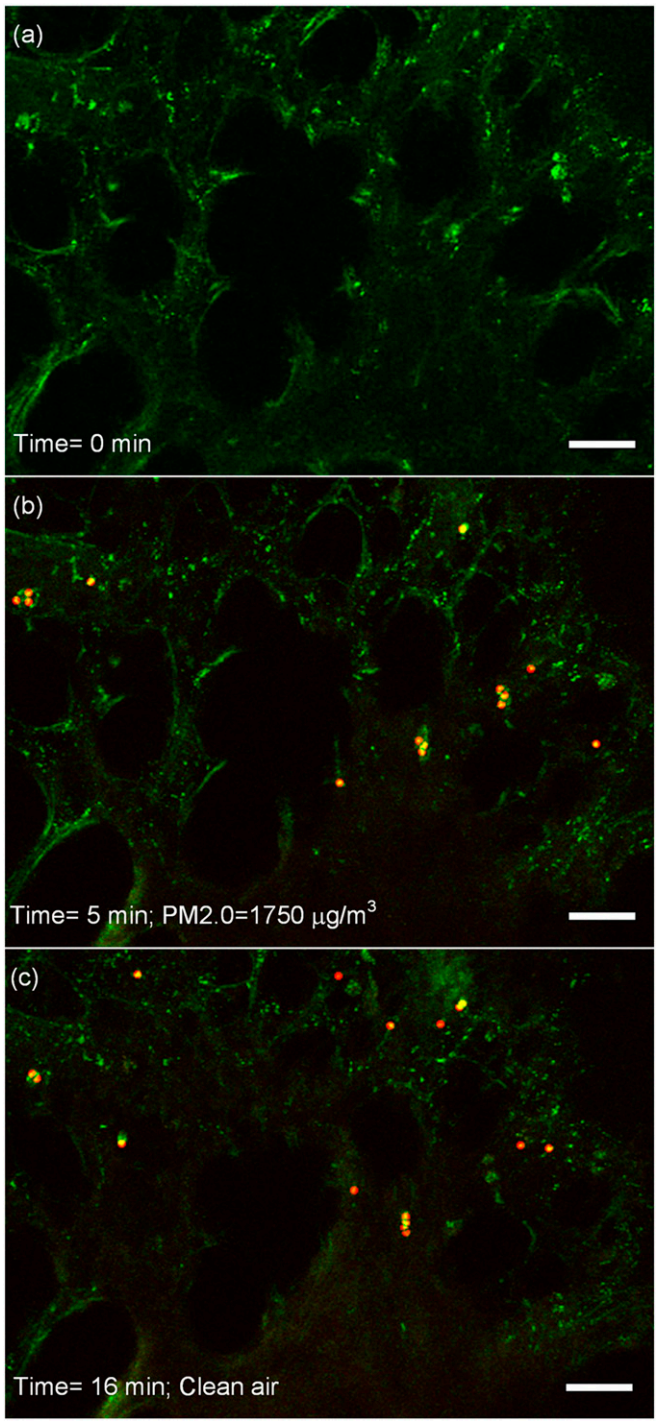

Fig. 2. The real-time observation on the deposition of $PM_{2.0}$. The tissue has a green color, while the red and yellow dots are the particles. (*A*) The acinar region before the ventilation of particles, and no particles are seen. (*B*) The deposition of $PM_{2.0}$ in the area at 5 min under the $PM_{2.0}$ level of 1,750 $\mu g/m^3$. (*C*) The deposition of $PM_{2.0}$ in the area at 16 min. At this moment, the $PM_{2.0}$ level is 0 $\mu g/m^3$, and the clean air has already been ventilated for 1 min. The scale bars in the images are 20 μm. The video of the deposition process is provided in Movie S1. The deposition process of $PM_{0.2}$ is also measured, and the images are provided in *SI Appendix*, Fig. S3.

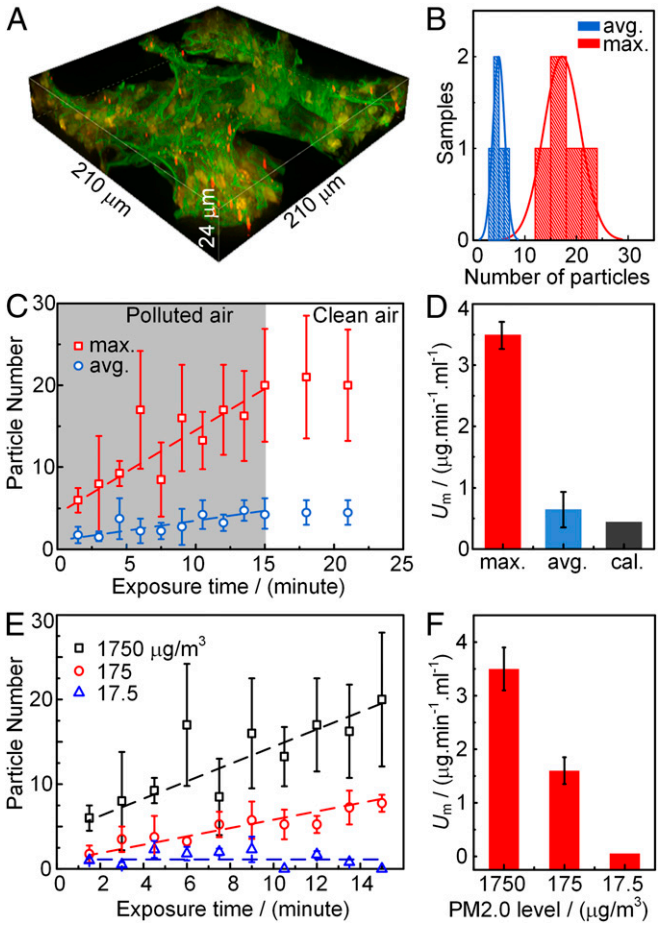

Fig. 3. The deposition rates of $PM_{2.0}$ in the selected local areas. (*A*) The 3D image of the $PM_{2.0}$ in a local area. (*B*) The statistic particle number in the local areas in the high-concentration region (max.) and in the medium concentration region (avg.) in 15 min. (*C*) The maximum and average deposition rates of $PM_{2.0}$ in the two local areas. The dash lines are the best fitting of the deposition rate in the polluted air condition with $PM_{2.0}$ level of 1,750 μg/m^3. (*D*) The maximum (max.) and average (avg.) mass deposition rates of $PM_{2.0}$ compared with the calculated (cal.) mass deposition rate from the average deposition model. (*E*) The maximum deposition rates of $PM_{2.0}$ in the local area under three $PM_{2.0}$ levels. (*F*) The maximum deposition rates of $PM_{2.0}$ under three $PM_{2.0}$ levels.

calculated deposition rate in Fig. 3*D*. The calculated deposition rate agrees well with the average deposition rate, but it is much lower than the maximum deposition rate. Therefore, the average deposition model can still be used to predict the average deposition rate in the acinar region, but the prediction is much lower than the maximum deposition rate in the high-concentration regions when the deposition pattern is nonuniform.

The deposition rate is also affected by the $PM_{2.5}$ levels in the air. The $PM_{2.5}$ level is the mostly concerned parameter of air pollution, especially in the countries with rapid development of industry in recent years. As shown in Fig. 3*E*, the deposition rate of the particle number is 0.38/min when $PM_{2.0}$ is 175 μg/m^3, and it increases to 0.8/min when $PM_{2.0}$ is 1,750 μg/m^3, while in good air quality condition that $PM_{2.0}$ is 17.5 μg/m^3, the number of the particles does not increase with the exposure time, the deposition rate is considered to be 0/min. The maximum mass deposition rates are shown in Fig. 3*F*, and they are compared with the published data of $PM_{2.5}$ deposition rates in the acinar region of human lungs measured in Nanjing (China) (20) and in Kolkata (India) (21). The $PM_{2.5}$ levels in Nanjing and Kolkata are 150~300 μg/m^3, and the calculated average deposition rates based on the ICRP model are 0.2~0.4 μg·min^{-1}·ml^{-1} and 0.15~0.25 μg·min^{-1}·ml^{-1}, respectively. The calculated average deposition rate is still much lower than the maximum deposition rate measured in our experiment at the $PM_{2.0}$ level of 175 μg/m^3. Thus, to determine the maximum deposition rate of $PM_{2.5}$ in acinar region, the real-time measurement is necessary instead of the calculation.

Particles in Extrapulmonary Organs. It is found that the deposited particles stay in the acinar region even when clean air is ventilated into the lung. They will finally be cleared by several mechanisms and pathways (22), which lead mainly to the gastrointestinal tract, the lymphatic system, and the blood circulation. The absorption of particles in blood circulation would lead to the deposition of particles in other important extrapulmonary organs. Actually, the transport of aerosol to an extrapulmonary organ has always been an important subject in health risk assessment and lung administration.

In the experiment, both $PM_{0.2}$ and $PM_{2.0}$ particles are found in the kidney and liver, as shown in Fig. 4. The $PM_{0.2}$ are found to aggregate in the medullary renal tubule of the kidney, as the red dots shown in Fig. 4*A1*. They are also found in the lobular sinus of the liver, as shown in Fig. 4*B1*. $PM_{0.2}$ are found in the kidney and liver of the other three mice under the $PM_{0.2}$ level of 1,750 μg/m^3, and the images are presented in *SI Appendix*, Fig. S4. Single particles of $PM_{2.0}$ are also found in the kidney and liver, but they are very few. For example, only one $PM_{2.0}$ particle is found in the kidney of a mouse, while one $PM_{2.0}$ particle is found in the liver of another mouse, as shown in Fig. 4 *C1* and *D1*. The single particles of $PM_{2.0}$ are found in the kidney and liver in other three mice, and they are presented in *SI Appendix*, Fig. S5. This is clear evidence that the $PM_{2.5}$ particles can enter the extrapulmonary organs. The details on the examination of the organ tissues are provided in the *Materials and Methods* section.

In the experiment, the particles are directly ventilated into the lung without passing other organs, and the connection between the intubation tube and the trachea was well sealed (described in the *Materials and Methods* section), thus the most possible pathway for the particles to enter the extrapulmonary organs is through the air-blood barrier in the acinar region. However, it is commonly accepted that only nanoparticles can pass through the air-blood barrier in the acinar region through the endocytosis or diffusion (23–26), while both the $PM_{0.2}$ and $PM_{2.0}$ particles are considered too large to pass through. One of the possible mechanisms is the internalization of particles by macrophages. Recent studies on incubation of polystyrene spheres with rat alveolar macrophages reveal that a macrophage attached to the polystyrene spheres with the size of 5 μm internalizes it in a few minutes (27).

Although the transport mechanism has not been clear yet, the deposition of the $PM_{0.2}$ and $PM_{2.0}$ particles in extrapulmonary organs is confirmed. It is attributed to the high detection resolution provided by the fluorescent method, so that the very small number of particles in the extrapulmonary organs can be detected, which used to need a long-term accumulation to a concentration high enough for the detection after an exposure for days or weeks.

Materials and Methods

In Vivo Inhalation Experiment. A mouse was anesthetized with Avertin (2,2,2-Tribromomethanol, FW282.7, Aldrich chemical T4,840–2, 20 mg/mL, 0.2 mL/10 g) intraperitoneally injected. It was then placed on a heated microscope stage with the aid of tape. A small incision was made in the trachea 3–4 mm below the throat, and a tracheal cannula was inserted. The other end of the cannula was connected to a mini ventilator (DW-3000C; ZS Dichuang Co.). The connection between the intubation tube and the trachea was well sealed, as shown by the schematics in Fig. 5. The mouse's breath was maintained by the mini ventilator with a tidal volume of 10 μL compressed

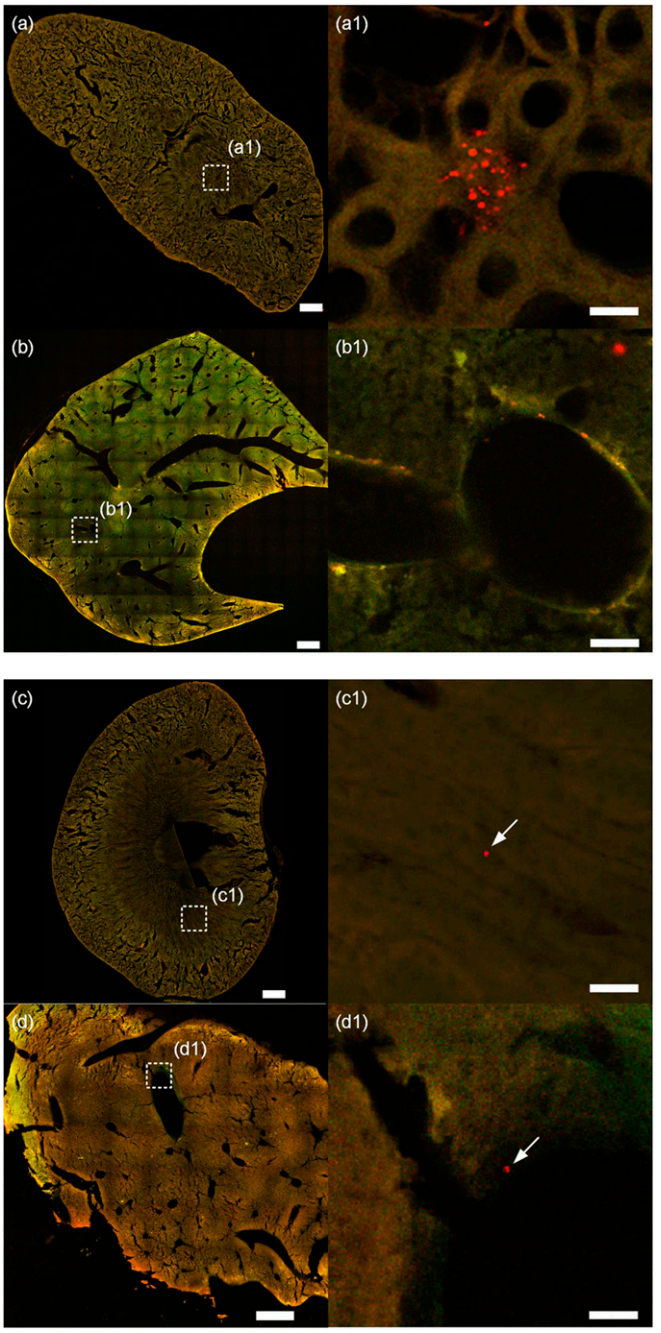

Fig. 4. Deposition of $PM_{0.2}$ and $PM_{2.0}$ particles in extrapulmonary organs. *A* and *B* are the cross-section of a kidney and liver, respectively, with the deposition of $PM_{0.2}$ particles. *A1* is the amplified image of the region marked in *A*. Red dots are fluorescent particles, and the back ground pattern is the structure of the medullary renal tubule of kidney. *B1* is the amplified image of the region in *B*. Fluorescent particles are found on the wall of the lobular sinus of the liver. *C* and *D* are the deposition of $PM_{2.0}$ on the cross-section of kidney and liver, respectively. *C1* is the amplified image of the region marked in *C*. A fluorescent particle is found on the background pattern of the medullary of the kidney. *D1* is the amplified image of the region marked in *D*. A red fluorescent particle is found on the wall of a lobular sinus of the liver. (The scale bars in *A*–*D* are 0.5 mm, in *A1* and *B1* are 10 μm, and in *C1* and *D1* are 20 μm.)

air (21% O_2) per gram of the mouse weight, and the respiratory rate was 120 breaths per minute, and a positive-end expiratory pressure of 2–3 cm H_2O. Fluorescent particles with the diameter of 0.2 and 2.0 μm were prepared in three different concentrations, and they were injected into the mouse lungs according to the tidal volumes and respiration rates. An inhalation experiment lasted for 15 min, and then, the aerosol was removed and clean air was ventilated into the lung for 10 min. The schematics of the experimental setup is shown in Fig. 5. For each experimental condition, i.e., each kind of particles in each concentration, five mice were tested.

A two-photon imaging microscope (FV1200MPE; Olympus Co.) was used to observe the deposition of particles in the mouse lung. The resolution of the microscope is 1 μm/pixel, and the scanning speed is 4 μs/pixel in an area of 512 × 512 pixels with a 25× objective lens. The mouse was laid in the left lateral decubitus status and a small surgical incision was made to expose the right rib cage. A second incision was then made into the intercostal space between ribs 3 and 4 through the parietal pleura to expose the lung. A custom flanged lung lobe fixator with an 8-mm circular coverslip was inserted between the two ribs. The suction with the pressure of 20–25 mmHg was applied to gently immobilize the lung. The objective lens of the two-photon imaging microscope was then placed over the thoracic window to observe the deposition of the particles in the acinar region of the lung.

Animals. Bal B/C mice (8 wk old) were purchased from laboratory animal research center of Tsinghua University, and they were applied for the experiments and kept in conventional conditions. All in vivo experiments were conducted in accordance with the Institute's Guide for the Care and Use of Laboratory Animals and were approved by the ethical committee of Tsinghua University (Approval No. 16#ZY-1).

Fluorescent Particles. Fluorescent dyed polystyrene particles with the diameter of 0.2 μm and 2 μm (R200 and R0200; Thermo Fisher Scientific) were respectively applied to simulate the PMs. The particles have an excitation wavelength of 542 nm with peak emission wavelength at 612 nm. Suspension was atomized by the aerosol generator in a 50 L sealed box. The concentration of the PMs in the air is $C = Q_L \times C_L \times \rho/Q_A$, where Q_L is the flow rate of the suspension, C_L is the concentration of particles in suspension, ρ is the density of the particles, and Q_A is the aerosol generation speed. In the experiment, Q_L = 0.2 mL/min, ρ =1.05 g/mL, Q_A = 6 L/min. $C_L = 5 \times 10^{-3}$% (vol/vol) for $PM_{0.2}$, $C_L = 5 \times 10^{-3}$%, 5×10^{-4}% and 5×10^{-5}% (vol/vol) for $PM_{2.0}$. Thus, the $PM_{2.0}$ concentrations are 1,750, 175, and 17.5 μg/m^3 in the air, respectively. The images of the particles from the aerosol is provided in the *SI Appendix*, Fig. S1. The concentration of the particles in the sealed box was monitored by a PM detector (DC1100-PRO-EMI; Dylos Co.), and the variation of the PMs level is provided in *SI Appendix*, Fig. S2.

Frozen Pieces of the Organs with Deposition Patterns. After the inhalation experiment, the mice were executed instantly by overdose intraperitoneally injection of Avertin. The lung, liver, and kidney were harvested and immersion-fixed in 10% neutral buffered paraformaldehyde for 24 h in the light-proof environment. All of the frozen sections were made under the lucifugal condition with the temperature of −20 °C. The fixed lung tissues were cut into 15 pieces through hilus pulmonis along the sagittal plane with the thickness of 100 μm for each piece. With the same method, three pieces of liver and three pieces of kidney along the sagittal plane were made.

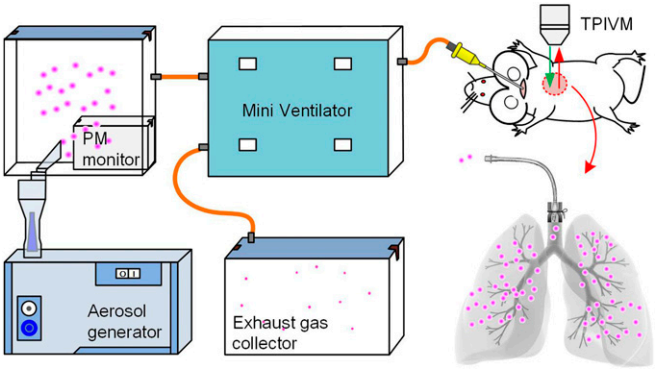

Fig. 5. Schematics of the inhalation experiment in vivo. This inhalation experiment system consists of PMs generator, PMs monitor, mini ventilation, and a two-photon imaging microscope. A small incision was made in the trachea 3–4 mm below the throat, and a tracheal cannula was inserted and well sealed by the suture.

The frozen sections were scanned under a laser confocal microscope (A1Rsi; Nikon Inc.). The emit wavelength was 542 nm. A 25× objective lens was used to scan the whole section of organs, and a 60× objective oil lens was used to observe the deposited particles in the local areas. The resolution of the microscope was 1.24 μm using the 25× lens, and 0.1 μm using the 60× lens. The 3D reconstruction of the deposition patterns of the particles in organs were carried out using Voloom/Imaris software (Bitplane AG).

Conclusion

In this work, a fluorescent imaging method is adopted in an inhalation experiment to observe the deposition of $PM_{2.5}$ in a mouse lung with high temporal and spatial resolutions. Therefore, the deposition rate of particles in a local area of interest in the acinar region can be directly measured. For $PM_{2.5}$ particles, which have a nonuniform deposition pattern, the measured maximum deposition rate is much higher than the predicted value from the widely used average deposition model.

Moreover, attributed to the high resolution of the fluorescent imaging method, single $PM_{0.2}$ and $PM_{2.0}$ particles are found in the kidney and liver. It is considered that the particles may pass through the air-blood barrier although the mechanism is not yet clear. The realization of the real-time observation on the deposition of the $PM_{2.5}$ in a local area of interest in lungs brings an insight to evaluate the risk of air pollution and to study the drug delivery efficiency of the inhalable drug particles in lung administration.

The data that support the findings of this study are available on request from the corresponding author H.C. The data are not publicly available due to them containing information that could compromise research, participant privacy, and consent.

ACKNOWLEDGMENTS. We thank Dr. Ruan Yingmao, Zhang Yanli, Dai Yali, and Cao Huizhen for their help in the experiments. This work is supported by Beijing Natural Science Foundation Grant 3172018 and National Natural Science Foundation of China Grants 51420105006 and 51322501.

1. Kaiser J (2005) Epidemiology. Mounting evidence indicts fine-particle pollution. *Science* 307:1858–1861.
2. Rattanapinyopituk K, et al. (2013) Ultrastructural changes in the air-blood barrier in mice after intratracheal instillations of Asian sand dust and gold nanoparticles. *Exp Toxicol Pathol* 65:1043–1051.
3. Pyne S (2002) Air pollution. Small particles add up to big disease risk. *Science* 295:1994.
4. Xu T, et al. (2018) Estimated individual inhaled dose of fine particles and indicators of lung function: A pilot study among Chinese young adults. *Environ Pollut* 235:505–513.
5. Raaschou-Nielsen O, et al. (2013) Air pollution and lung cancer incidence in 17 European cohorts: Prospective analyses from the European Study of Cohorts for Air Pollution Effects (ESCAPE). *Lancet Oncol* 14:813–822.
6. Kreyling WG, et al. (2014) Air-blood barrier translocation of tracheally instilled gold nanoparticles inversely depends on particle size. *ACS Nano* 8:222–233.
7. Roberts S, Martin MA (2007) Methods for bias reduction in time-series studies of particulate matter air pollution and mortality. *J Toxicol Environ Health A* 70:665–675.
8. Zhang Y, et al. (2015) Association between ambient air pollution and hospital emergency admissions for respiratory and cardiovascular diseases in Beijing: A time series study. *Biomed Environ Sci* 28:352–363.
9. Patton JS, Byron PR (2007) Inhaling medicines: Delivering drugs to the body through the lungs. *Nat Rev Drug Discov* 6:67–74.
10. International Commission on Radiological Protection (1994) *Human Respiratory Tract Model for Radiological Protection. ICRP Publication 66* (Elsevier Science, Tarrytown, NY).
11. Brunekreef B, Holgate ST (2002) Air pollution and health. *Lancet* 360:1233–1242.
12. Wolf K, et al. (2015) Long-term exposure to particulate matter constituents and the incidence of coronary events in 11 European cohorts. *Epidemiology* 26:565–574.
13. Fishler R, Hofemeier P, Etzion Y, Dubowski Y, Sznitman J (2015) Particle dynamics and deposition in true-scale pulmonary acinar models. *Sci Rep* 5:14071.
14. Tsuda A, Butler JP, Fredberg JJ (1994) Effects of alveolated duct structure on aerosol kinetics. II. Gravitational sedimentation and inertial impaction. *J Appl Physiol (1985)* 76:2510–2516.
15. Kumar H, Tawhai MH, Hoffman EA, Lin C-L (2011) Steady streaming: A key mixing mechanism in low-Reynolds-number acinar flows. *Phys Fluids (1994)* 23:41902.
16. Haber S, Yitzhak D, Tsuda A (2003) Gravitational deposition in a rhythmically expanding and contracting alveolus. *J Appl Physiol (1985)* 95:657–671.
17. Hofemeier P, Fishler R, Sznitman J (2014) The role of respiratory flow asynchrony on convective mixing in the pulmonary acinus. *Fluid Dyn Res* 46:041407.
18. Stahlhofen W, Rudolf G, James A (1989) Intercomparison of experimental regional aerosol deposition data. *J Aerosol Med* 2:285–308.
19. Haefeli-Bleuer B, Weibel ER (1988) Morphometry of the human pulmonary acinus. *Anat Rec* 220:401–414.
20. Wang G, Huang L, Gao S, Gao S, Wang L (2002) Measurements of PM10 and PM2.5 in urban area of Nanjing, China and the assessment of pulmonary deposition of particle mass. *Chemosphere* 48:689–695.
21. Nag S, Gupta AK, Mukhopadhyay UK (2005) Size distribution of atmospheric aerosols in Kolkata, India and the assessment of pulmonary deposition of particle mass. *Indoor Built Environ* 14:381–389.
22. Lippmann M, Yeates DB, Albert RE (1980) Deposition, retention, and clearance of inhaled particles. *Br J Ind Med* 37:337–362.
23. Kwon JT, et al. (2008) Body distribution of inhaled fluorescent magnetic nanoparticles in the mice. *J Occup Health* 50:1–6.
24. Sarlo K, et al. (2009) Tissue distribution of 20 nm, 100 nm and 1000 nm fluorescent polystyrene latex nanospheres following acute systemic or acute and repeat airway exposure in the rat. *Toxicology* 263:117–126.
25. Murugan K, et al. (2015) Parameters and characteristics governing cellular internalization and trans-barrier trafficking of nanostructures. *Int J Nanomedicine* 10:2191–2206.
26. Heyder J, Gebhart J, Rudolf G, Schiller CF, Stahlhofen W (1986) Deposition of particles in the human respiratory-tract in the size range 0.005-15-Mu-M. *J Aerosol Sci* 17:811–825.
27. Champion JA, Mitragotri S (2006) Role of target geometry in phagocytosis. *Proc Natl Acad Sci USA* 103:4930–4934.